Journal of Power Sources 236 (2013) 39–46

Contents lists available at SciVerse ScienceDirect

Journal of Power Sources

journal homepage: www.elsevier.com/locate/jpowsour

Short communication

Beneficial influence of succinic anhydride as electrolyte additive on the self-discharge of 5 V $LiNi_{0.4}Mn_{1.6}O_4$ cathodes

Vasily Tarnopolskiy [a,b], Julian Kalhoff [a], Martina Nádherná [a], Dominic Bresser [a,*], Lionel Picard [b], Frédéric Fabre [b], Marlène Rey [b], Stefano Passerini [a,*]

[a] Institute of Physical Chemistry and MEET Battery Research Centre, University of Muenster, Corrensstr. 28/30 & 46, 48149 Muenster, Germany
[b] CEA/LITEN, Commissariat a l'Energie Atomique/Laboratoire d'Innovation pour les Technologies des Energies Nouvelles, 17 rue des Martyrs, 38054 Grenoble Cedex 9, France

HIGHLIGHTS

- Self-discharge mechanism of high voltage lithium-ion battery cathodes.
- Surface film formation on high voltage cathodes by electrolyte additives.
- Improved performance of $LiNi_{0.4}Mn_{1.6}O_4$ by using succinic anhydride as electrolyte additive.

ARTICLE INFO

Article history:
Received 11 October 2012
Received in revised form
30 January 2013
Accepted 2 February 2013
Available online 19 February 2013

Keywords:
$LiNi_{0.4}Mn_{1.6}O_4$
Succinic anhydride
Additive
Self-discharge
5 V lithium-ion cathode

ABSTRACT

The self-discharge mechanism of $LiNi_{0.4}Mn_{1.6}O_4$, investigated by electrochemical methods, is mostly attributed to oxidative electrolyte decomposition due to the high lithium (de-)insertion potentials, since the material insertion capacity appears to be fully reversible upon subsequent galvanostatic cycling. A series of 40 different compounds, such as for instance fluorinated ethylene carbonate, 1,3-propane sultone, lithium bis(oxalato)borate (LiBOB), or a variety of ionic liquids, was investigated as suitable electrolyte additives to form a stable LNMO/electrolyte interphase in order to prevent the self-discharge by the continuous oxidative electrolyte decomposition. Among these, only one compound, namely succinic anhydride, revealed to have a beneficial effect on the self-discharge of LNMO based cathodes, while showing an enhanced coulombic efficiency and a decreased capacity loss per cycle. Additionally, the modification of the LNMO particles surface by adding succinic anhydride to the electrolyte was confirmed by performing *ex situ* SEM and XPS analysis of galvanostatically cycled electrodes.

1. Introduction

Transition metal-substituted lithium manganese oxides, as for instance $LiNi_{0.5}Mn_{1.5}O_4$, having a spinel-type structure, firstly reported by Amine et al. [1] and Dahn et al. [2], are currently considered as one of the most promising high voltage cathodes for future lithium-ion batteries, due to their inherent high conductivity and advanced rate capability [3–8]. More importantly, these oxides generally offer operating potentials >4.5 V and thus, an increased overall cell voltage, which results in enhanced energy densities of the resulting lithium-ion cells.

Regarding $LiNi_{0.5}Mn_{1.5}O_4$, several studies have revealed that the disordered phase (*Fd-3m*) shows superior electrochemical performance compared to the ordered phase ($P4_332$) [7–9]. However, based on a long-term structural and electrochemical investigation of nickel substituted lithium manganese oxide spinels, Patoux et al. [8,10] have identified $LiNi_{0.4}Mn_{1.6}O_4$ (hereinafter named LNMO), comprising a reduced content of nickel, as further improved electrode material relatively to disordered $LiNi_{0.5}Mn_{1.5}O_4$, particularly in terms of practical energy density at elevated applied current densities.

Nevertheless, the highly attractive lithium insertion potential of 4.7–4.75 V of such materials turns out as a major challenge with respect to the limited electrochemical stability window of common liquid, organic solvent-based electrolytes. Accordingly, the carbonate electrolytes are oxidatively decomposed at the cathode surface upon high operating potentials, leading to continuous electron transfer from the electrolyte to the cathode and, simultaneously, a Li^+ ion re-insertion, resulting in rather poor coulombic efficiencies [4,5,10–13].

Possible strategies to overcome this issue comprise the utilization of ionic liquids as electrolyte solvent due to the generally

* Corresponding authors.
E-mail addresses: dominic.bresser@uni-muenster.de (D. Bresser), stefano.passerini@uni-muenster.de (S. Passerini).

0378-7753/$ – see front matter © 2013 Elsevier B.V. All rights reserved.
http://dx.doi.org/10.1016/j.jpowsour.2013.02.030

enhanced anodic stability of ionic liquid-based electrolytes relatively to common liquid carbonate-based electrolytes [14]. However, ionic liquids suffer from poor conductivity, thus affecting the enhanced high rate performance of $LiNi_{0.5}Mn_{1.5}O_4$. Another approach has been the avoidance of electrolyte-active material contact by coating the $LiNi_{0.5}Mn_{1.5}O_4$ particles, for instance, with ZnO [15–17], ZrO_2 [18], carbon [19], or as very recently reported with $LiFePO_4$ [20]. Although such surface modifications have turned out to be a rather promising approach to protect or passivate the highly reactive $LiNi_{0.5}Mn_{1.5}O_4$ particles surface, these mostly post-synthesis approaches are not very attractive for large-scale commercial applications.

A more facile and economically effective way of modifying the electrode–electrolyte interphase is certainly the utilization of electrolyte additives, as for carbonaceous anode materials [21]. However, only a few additives have been so far identified to be suitable for high voltage $LiNi_{0.5}Mn_{1.5}O_4$ cathodes, including *inter alia* tris(hexafluoro-*iso*-propyl)phosphate [22], lithium bis(oxalate) borate [23], 1,3-propane sultone [10], or glutaric anhydride [24]. Interestingly, Lee et al. [25] reported in 2007 an improved cycling stability and reduced swelling behavior for a $LiNi_{0.5}Mn_{1.5}O_4$/graphite lithium-ion full cell using a combination of 1,3-propane sultone and succinic anhydride, a derivative of glutaric anhydride, as electrolyte additives. They concluded that the improved cycling stability would originate from the SEI-forming ability of these additives on graphite and their electrochemical stability on the cathode toward high potentials.

However, based on the results reported hereinafter, utilizing succinic anhydride (SA) as electrolyte additive within LNMO/Li half-cells, we will show that the improved performance mainly results from its beneficial influence on the LNMO-electrolyte interphase. As a matter of fact, we demonstrate in here that by adding several percent of SA to the base electrolyte, the self-discharge and the coulombic efficiency can be significantly reduced and enhanced, respectively.

2. Experimental

2.1. $LiNi_{0.4}Mn_{1.6}O_4$ synthesis

The $LiNi_{0.4}Mn_{1.6}O_4$ active material was synthesized by a high temperature solid state method [8,10]. In brief, stoichiometric amounts of the corresponding carbonates (Li_2CO_3, $NiCO_3 \times 2\,Ni(OH)_2 \times xH_2O$, and $MnCO_3$) were mechanically mixed by means of ball-milling in hexane. After the subsequent thermal treatment for 10 h at 600 °C and 15 h at 900 °C (applied cooling rate $\approx 1.0\,^{\circ}C\,min^{-1}$) the resulting particles were dispersed in aqueous solution to separate agglomerated particles. The pristine particles morphology and structure were characterized by performing high resolution scanning electron microscopy (HRSEM), utilizing a ZEISS Auriga® microscope. The final composition of the as synthesized LNMO active material was determined by performing inductively coupled plasma optical emission spectrometry (ICP-OES, SPECTRO ARCOS).

2.2. Electrode preparation

Electrodes based on $LiNi_{0.4}Mn_{1.6}O_4$ (LNMO) were prepared, comprising 85 wt.% of LNMO, 10 wt.% of conductive carbon (Super C65®, TIMCAL), and 5 wt.% PVdF (Solef 5130, SOLVAY). N-methyl-pyrrolidinone (SIGMA-ALDRICH) was used as the solvent. The mixture was homogenized by planetary ball milling at 800 rpm for 2 h (Vario-Planetary Mill Pulverisette 4, FRITSCH). The obtained slurry was subsequently casted on aluminum foil (EVONIK, 20 μm, purity > 99.9%) utilizing a laboratory doctor blade with a wet film thickness of 400 μm. The resulting electrode sheets were pre-dried at 80 °C for 12 h under ambient atmosphere and additionally for 12 h at 120 °C under vacuum. The thus dried electrodes were pressed by utilizing a HOHSEN calendaring machine, resulting in an effective reduction of the coating thickness of 25–30%. Subsequently, disk electrodes ($ø = 12$ mm) were punched and dried again at 120 °C for 12 h under vacuum. The active material mass loading was comprised between 9.5 and 10.5 mg cm^{-2}, having a final thickness of 80–85 μm, including the thickness of the aluminum current collector.

2.3. Electrochemical characterization

All electrochemical studies were performed utilizing three-electrode, Swagelok™-type cells. As counter and reference electrodes lithium metal foils (Rockwood Lithium, battery grade) were used. Hence, all potential values reported in this manuscript refer to the Li^+/Li reference couple. Cells were assembled in a MBraun glove box with a water and oxygen content of less than 0.5 ppm, using a Whatman GF/D borosilicate glass microfiber filter as separator, drenched with a solution of 1 M $LiPF_6$ in a 1:1 volume mixture of ethylene carbonate (EC) and dimethyl carbonate (DMC) (LP30, MERCK) as electrolyte. All electrochemical studies were performed at 20 (±1) °C. Galvanostatic experiments were performed by means of a Maccor Battery Tester 4300.

Self-discharge studies were performed analog to the following testing protocol: five formation cycles at C/2, charge to a cut-off potential of 4.95 V with an applied C rate of C/2 and a subsequent CV step to C/20. Then the cells were left under OCV conditions for 99 h (first checkpoint, potential decay) and subsequently charged again at C/2 (second checkpoint, lost specific capacity corresponding to the voltage decay) before the cell was cycled for 50 additional cycles at C/2.

2.4. Ex situ characterization of cycled $LiNi_{0.4}Mn_{1.6}O_4$ based electrodes

For the *ex situ* SEM analysis of cycled LNMO-based electrodes, cells containing LP30 as electrolyte and a varying content of SA were cycled according to the following protocol: 3 formation cycles at C/10//D/10, 5 cycles at C/5//D/5, each 1 cycle at C/5//10D, C/5//D/5, 10C//D/5, and C/5//D/5, and finally 50 cycles at 1C//1D. The charge/discharge rate of 1C/1D corresponds to an applied current of 146 mA per gram of active material. Subsequently, the cells were disassembled in a MBraun glove box. The electrodes were rinsed twice with DMC and dried inside the glove box. The thus prepared electrodes were then transferred to the HRSEM antechamber for further analysis using a modified sample holder to prevent contact to air and moisture.

Ex situ X-ray photoelectron spectroscopy (XPS) on LNMO-based electrodes was carried out using an Axis Ultra HAS spectroscope (KRATOS) equipped with a monochromatic Al K_α source at 10 mA and 12 kV. The measurements were performed with a pass energy of 20 eV. A charge neutralizer was used to compensate the charging of the samples. The analysis area on the sample surface was about 300 μm × 700 μm. LNMO based electrodes were galvanostatically cycled analogously to the self-discharge protocol, as already described. The electrodes were subsequently transferred to the ante-chamber under argon atmosphere in order to avoid the contact to oxygen and moisture and were not rinsed prior to the XPS analysis in order to prevent a possible dissolution of the SEI. For the comparative evaluation of the obtained spectra, energy indication and component fitting were calibrated according to the peak for amorphous carbon in the C 1s spectra, due to the presence of carbon black (Super C65®) in all of the investigated samples and its characteristic binding energy of 285 eV.

3. Results and discussion

In Fig. 1, SEM images of the as-synthesized $LiNi_{0.4}Mn_{1.6}O_4$ particles are presented showing well-crystallized particles with an average diameter of 3–5 μm. Such particle size and morphology appears preferable, as recent comparative investigations on disordered $LiNi_{0.5}Mn_{1.5}O_4$, having different sizes and morphologies, revealed a superior electrochemical performance in terms of cycling stability as well as high rate capability for well crystallized, micro-sized particles [26,27]. In fact, previous reports on the herein investigated material have presented an enhanced high rate performance for very similar LNMO particles [10]. The Li:Mn:Ni ratio was determined to be 1:1.59:0.36 by performing ICP-OES analysis, which will be indicated as $LiNi_{0.4}Mn_{1.6}O_4$ or, simply, LNMO hereinafter.

As mentioned previously, one of the most critical issues regarding the application of spinel structured, nickel doped, lithium manganese oxide as high voltage cathode material for a new generation of high energy lithium-ion batteries, is the self-discharge upon storage at fully charged state. Hence, in order to investigate this self-discharge behavior more in detail, electrodes were prepared and LNMO half-cells were assembled. In a first step, a LNMO half-cell was charged to a cut-off potential of 4.95 V (100% SOC) after three initial formation cycles at C/10 and kept under OCV conditions for more than 30 days, while the cell potential was recorded (Fig. 2, curve a). The potential of the cell decreased rapidly to *ca.* 4.73 V and then, more slowly, to *ca.* 4.67 V. However, as for the subsequent charge/discharge cycles (not shown) the typical specific capacities could be obtained, the observed self-discharge was considered to be mostly reversible, which is in good agreement with the results reported by Yazami and Ozawa [12] on the self-discharge of $LiMn_2O_4$ based electrodes.

For an easier comparison, the typical discharge profile of LNMO at low C rates is also included in Fig. 2 (curve b). It is obvious that both cells are following a similar potential profile, indicating that both processes follow a similar mechanism. In fact, the self-discharge was already proposed to derive from a lithium re-insertion from the electrolyte, according to the following scheme [12,28–30]:

$$Li_aNi_{0.4}Mn_{1.6}O_4 + b{*}Li^+ + b{*}e^- \rightarrow Li_{a+b}Ni_{0.4}Mn_{1.6}O_4$$

This reversible re-insertion is suggested to be mainly driven by the oxidative electrolyte decomposition at high voltages, leading to an electron transfer to the active material, requiring a concomitant lithium re-insertion in order to maintain the charge neutrality [12,28,29], as schematically illustrated in Fig. 3.

In order to determine the resulting current released by the observed self-discharge at a specific potential, in a second step, LNMO half-cells were charged and discharged in potentiostatic steps (ΔU = 0.05 V; each potential was kept constant for 5 h). Recording the required current, called float-current, to counterbalance the ongoing self-discharge process allows to determine the self-discharge current, assuming the self-discharge to be fully reversible (Fig. 4) [29,31]. It appears obvious, that the float-current is highly dependent on the applied potential and independent of the fact, whether the electrode is currently charged or discharged. Moreover, it is observed that the float-current rapidly increases for applied potentials higher than 4.5 V. Such a rapid increase of the float-current was already reported by Yang et al. [32] on the oxidative decomposition of carbonate based electrolytes on lithium-free $Ni_{0.5}Mn_{1.5}O_3$ and further confirms the proposed self-discharge mechanism schematically illustrated in Fig. 3, based on the oxidative decomposition of the electrolyte at elevated potentials and concomitant lithium re-insertion.

However, as the observed self-discharge appears only as the symptom, strategies to overcome this issue will certainly have to

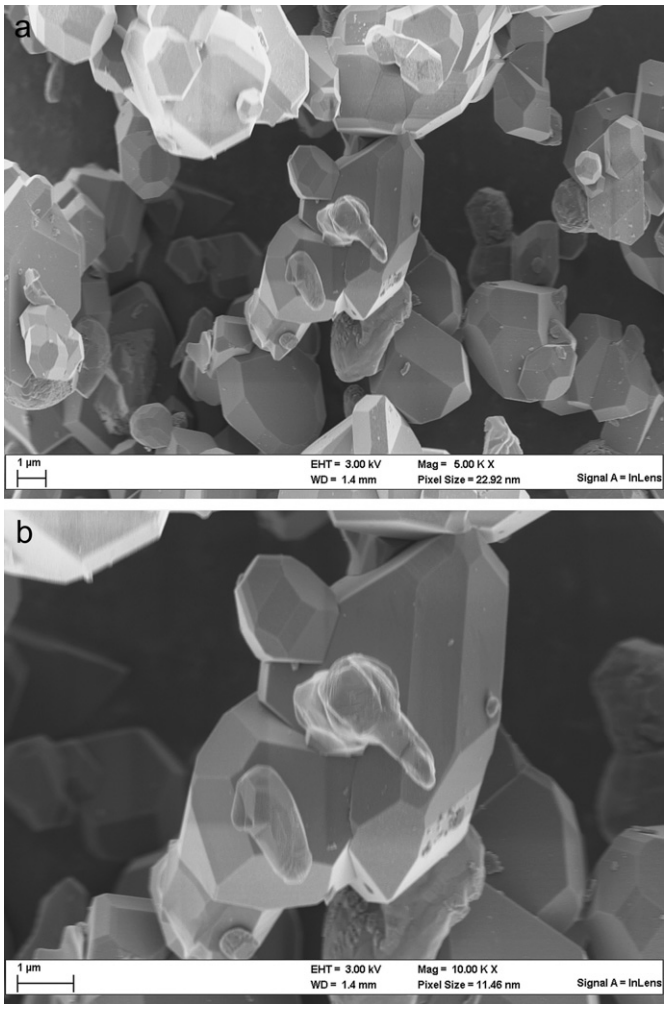

Fig. 1. SEM images of the as synthesized LNMO particles at different magnifications.

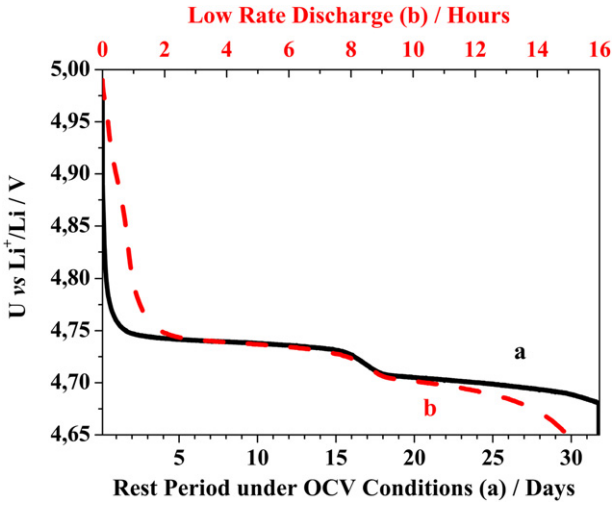

Fig. 2. Voltage profiles of two LNMO half-cells, one stored at the fully charged state (SOC 100, 4.95 V) for more than 30 days (curve a, solid line) and one discharged at low C rates (curve b, dashed line).

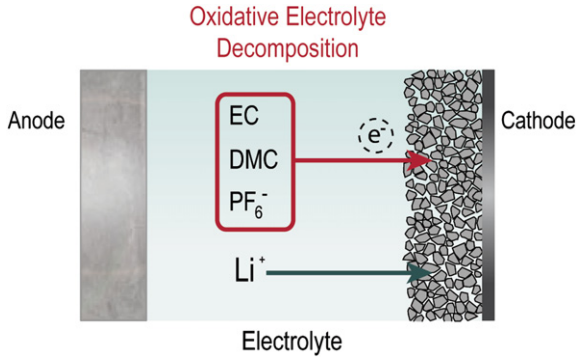

Fig. 3. Schematic illustration of the oxidative electrolyte decomposition at the cathode surface at high potentials and the concomitant lithium re-insertion.

address its origin – the ongoing decomposition of the electrolyte at the cathodes surface. This is particularly important considering the limited amount of electrolyte in commercial lithium-ion cells, in which the electrolyte decomposition would lead to drying-out, concomitant rapid capacity fading and increase of the internal pressure, if gaseous products are formed. Additionally, the soluble electrolyte decomposition products might affect the performance of the negative electrode [13,33].

The most promising and efficient strategy for inhibiting the continuous electrolyte decomposition at the cathodes surface is certainly the creation of a solid electrolyte interphase (SEI) analogous to that formed on the graphite surface (Fig. 5) [3,34,35]. Hence, a series of 40 different compounds in various concentrations (Table 1) were studied as electrolyte additives with respect to their potential film forming characteristics on the high voltage cathode material, according to the testing protocol described in Section 2.3.

Among all the additives tested, only one had a significant beneficial effect on the self-discharge behavior of LNMO based electrodes, succinic anhydride (Fig. 6). Other additives, including several derivatives of succinic anhydride, simply had no effect on the self-discharge, others had an even detrimental impact (see Table 1) as the one exemplary shown in Fig. 6 (solid dots). Nevertheless, it appeared that by increasing the amount of added succinic anhydride (SA), the self-discharge in terms of potential decay could be further reduced (checkpoint 1, indicated by the black arrow in Fig. 6). In order to quantify the self-discharge effect in terms of "lost" capacity (checkpoint 2), the cells were subsequently charged

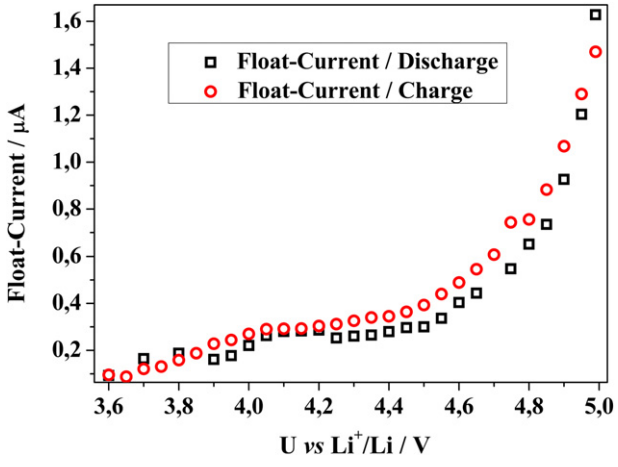

Fig. 4. Float-current recorded upon stepwise potentiostatic (ΔU = 0.05 V; each potential was kept constant for 5 h) charge and discharge of an LNMO electrode.

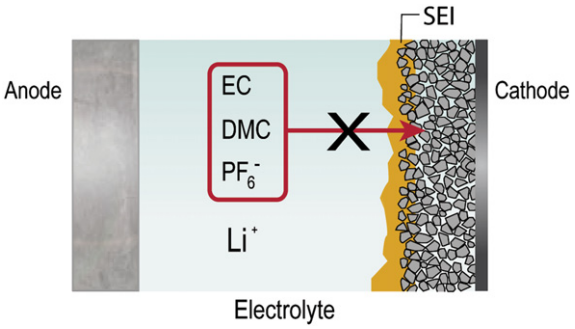

Fig. 5. Schematic illustration of a protective SEI layer on the cathode surface, inhibiting further oxidative electrolyte decomposition and thus, lithium re-insertion.

again to the upper cut-off potential of 4.95 V. As a matter of fact, for cells comprising pure LP30 as electrolyte, a specific capacity of around 13.5 mAh g^{-1} could be obtained for this subsequent charge step, while it was only around 9.5, 8.4, and 6.6 mAh g^{-1} for those cells comprising 1%, 2%, and 8% of SA as electrolyte additive,

Table 1
Enumeration of the tested compounds and the corresponding percentage in the base electrolyte solution (1 M $LiPF_6$ in EC:DMC, 1:1). The tendency of the influence on the self-discharge is indicated by '+', '0', or '–' for a beneficial, almost none, or a detrimental effect, respectively.

	Tested compound	Concentration of additive/%	Influence on self-discharge
1	Poly(ethylene glycol) methylether methacrylate	0.5; 1; 4	–
2	Methyl allyl piperidinium-1,3 TFSI	1; 5; 20	–
3	Methylmethacrylate	1	–
4	Pyrrole	1	– –
5	Biphenyl	0.1	–
6	Methyl allylpyrrolidinium FSI	5	– –
7	Methyl allylpyrrolidinium BF_4	1; 5	–
8	Tetrahydrothiophene	4	0
9	3-Bromo-4-methoxy benzonitrile[a]	1	–
10	4,4′-Dimethoxyoctafluorobiphenyl[a]	1	–
11	5-Chloro-2-methoxypyridine[a]	1	– –
12	Fluoroethylene carbonate	4	0
13	Difluoroethylene carbonate	4	0
14	Trifluoroethylene carbonate	4	–
15	Bis(trifluoromethyl)ethylene carbonate	4	0
16	1,3-Propane sultone	4	0
17	Tris(trimethylsilyl)borate	2; 5	0
18	Tris(trimethylsilyl)phosphite	2; 5	0
19	Trimethylsilyltriflate	4	–
20	Bis(trimethylsilyl)malonate	4	–
21	Ethylmethylsulfone	4	0
22	Dimethyl sulfone	4	0
23	Methyl methanesulfonate	4	0
24	Sulfolane	4	0
25	1,3,2-Dioxathiolane 2,2-dioxide	4	– –
26	Tetramethoxytitanium	4	–
27	1,2-Propyleneglycol sulfite	4	–
28	Lithium bis(oxalate)borate (LiBOB)	4	–
29	Lithium difluoro(oxalate)borate	4	–
30	Tetrafluorosuccinic anhydride	4	–
31	Ethylene sulfite	4	–
32	Succinic anhydride	1; 2; 4; 6; 8	+ +
33	Methyl succinic anhydride	0.5; 4; 8	0 to +
34	Diglycolic anhydride	6	–
35	Maleic anhydride	1; 4	–
36	2,2-Dimethyl succinic anhydride	1	0
37	2-(Trifluoroacetamido) succinic anhydride	0.5	–
38	2-Methylene succinic anhydride	0.5	–
39	Nonenylsuccinic anhydride	0.5	– –
40	Dodecenylsuccinic anhydride	0.5	– –

[a] Proposed as electrolyte additives for overcharge protection with an oxidation potential of >4.5 V [48].

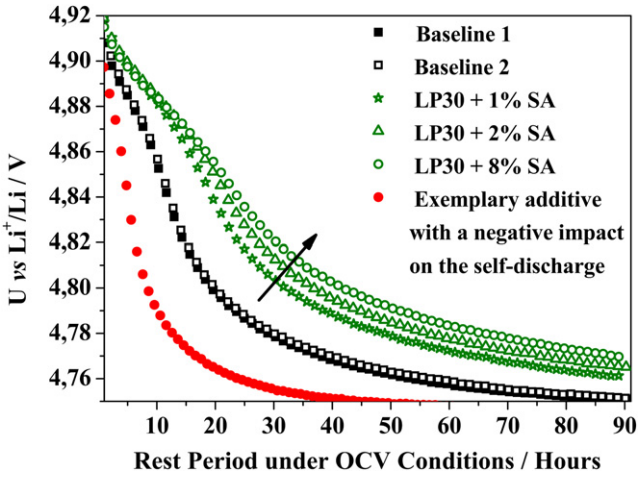

Fig. 6. Potential profiles of LNMO half-cells, kept under OCV conditions after having been fully charged (SOC 100, 4.95 V) for 99 h. Black curves: baseline 1 and 2, LP30 only. Red curve: exemplary curve for a half-cell comprising LP30 and an additive with a negative impact on the self-discharge. Green curves: LNMO half-cells, comprising 1%, 2%, and 8% of SA as electrolyte additive, increasing effect for increasing amount of additive (indicated by the black arrow). (For interpretation of the references to color in this figure legend, the reader is referred to the web version of this article.)

respectively. This result is particularly surprising as Lee et al. [25] did not observe any oxidative decomposition of SA on a platinum electrode toward applied potentials up to 6.0 V upon performing linear sweep voltammetry and hence concluded, that SA would have no effect on the $LiNi_{0.5}Mn_{1.5}O_4$ cathode, but act as a SEI stabilizing additive on the graphite anode. Indeed, plotting the differential capacity (dQ/dV) for the first cycle of those cells comprising pure LP30 and LP30 + 2% of SA as electrolyte (Fig. 7) does not indicate any electrochemically induced oxidative decomposition of SA toward elevated potentials. Only the characteristic features corresponding to the oxidation and reduction of manganese, from 3.84 to 4.4 V, and nickel, from 4.5 to 4.8 V, are observed [10,36].

However, as previously reported [11,37–39], the presence of transition metals in the cathode might catalyze the oxidative decomposition of SA and the evolving current might not be detectable due to an overlapping with the anodic peaks for the oxidation of manganese and nickel. Moreover, as SA obviously

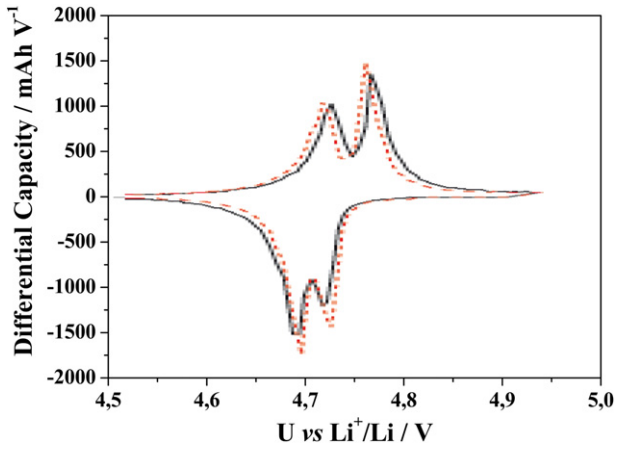

Fig. 7. Differential capacity plot (dQ/dV) of the first cycle at C/2 for LNMO based half-cells, comprising pure LP30 (black curve) and LP30 + 2% of SA (red dashed curve) as electrolyte in the voltage range from 4.5 to 4.95 V. (For interpretation of the references to colour in this figure legend, the reader is referred to the web version of this article.)

allows a reduction of the self-discharge on the LNMO cathode up to 50%, it must have a beneficial influence on the LNMO/electrolyte interphase. This beneficial impact is further indicated by improvements of coulombic efficiency and cycling stability of LNMO based cathodes, as revealed by the continuous constant current cycling at C/2 (Fig. 8a). The capacity loss per cycle in presence of 4% SA decreased to only 0.001% (versus 0.047% in pure LP30, Fig. 8b), the coulombic efficiency increased to around 99.6% (versus 99.4%, Fig. 8b) and, finally, a stable specific capacity of around 136 mAh g^{-1}. Regarding the coulombic efficiency it should be pointed out that even the modest improvement from 99.4% to 99.6% results in a significantly enhanced capacity retention of a full lithium-ion cell comprising an LNMO-based cathode. In fact, a full cell using the SA additive would theoretically deliver 82% and 67% of its initial capacity after 50 and 100 cycles, respectively. However, a coulombic efficiency of 99.4% would result in a capacity retention of only 74% and 55% after 50 and 100 cycles, respectively. It is then reasonable to assume that the addition of SA decreases electrolyte decomposition, resulting in an improved coulombic efficiency [26], although the formation of a SEI from the decomposition of SA is not directly observable from electrochemical measurements.

For a further investigation of the LNMO surface, *ex situ* HRSEM analysis of electrodes cycled in pure LP30 (Fig. 9c, d), and LP30 with 4% (Fig. 9e, f) and 8% of SA (Fig. 9g, h) as electrolyte, was performed and compared with pristine electrodes (Fig. 9a, b). Obviously, some of the particles show rougher and partially broken edges (Fig. 9a, b) compared to the pristine powder (Fig. 1), likely caused by the ball-milling for the slurry dispersion and subsequent calendaring upon electrode preparation. Nevertheless, the large cracks observed

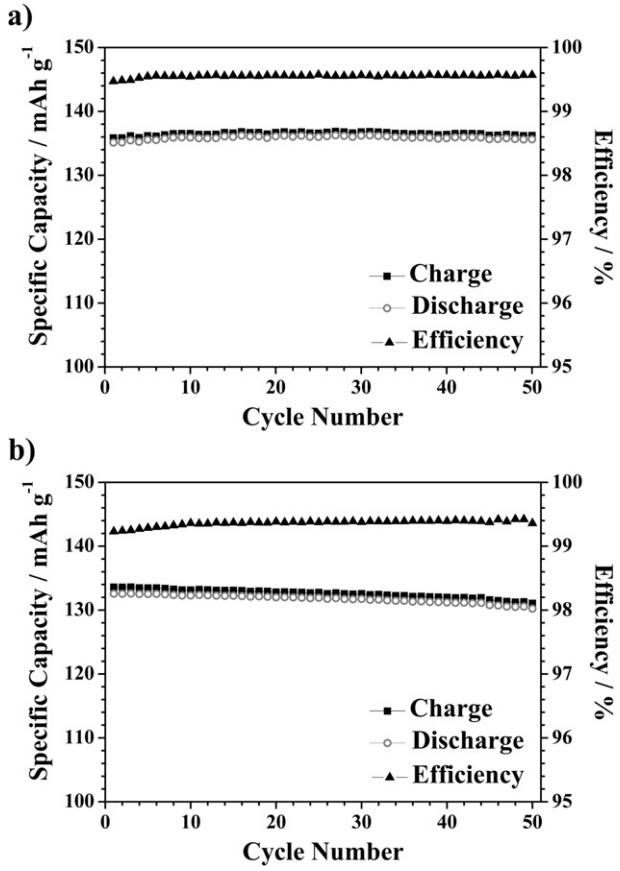

Fig. 8. Continuous constant current cycling of an LNMO based electrode at C/2, comprising a) 4% of SA in LP30 and b) pure LP30. Cut-off potentials: 3.5 and 4.95 V.

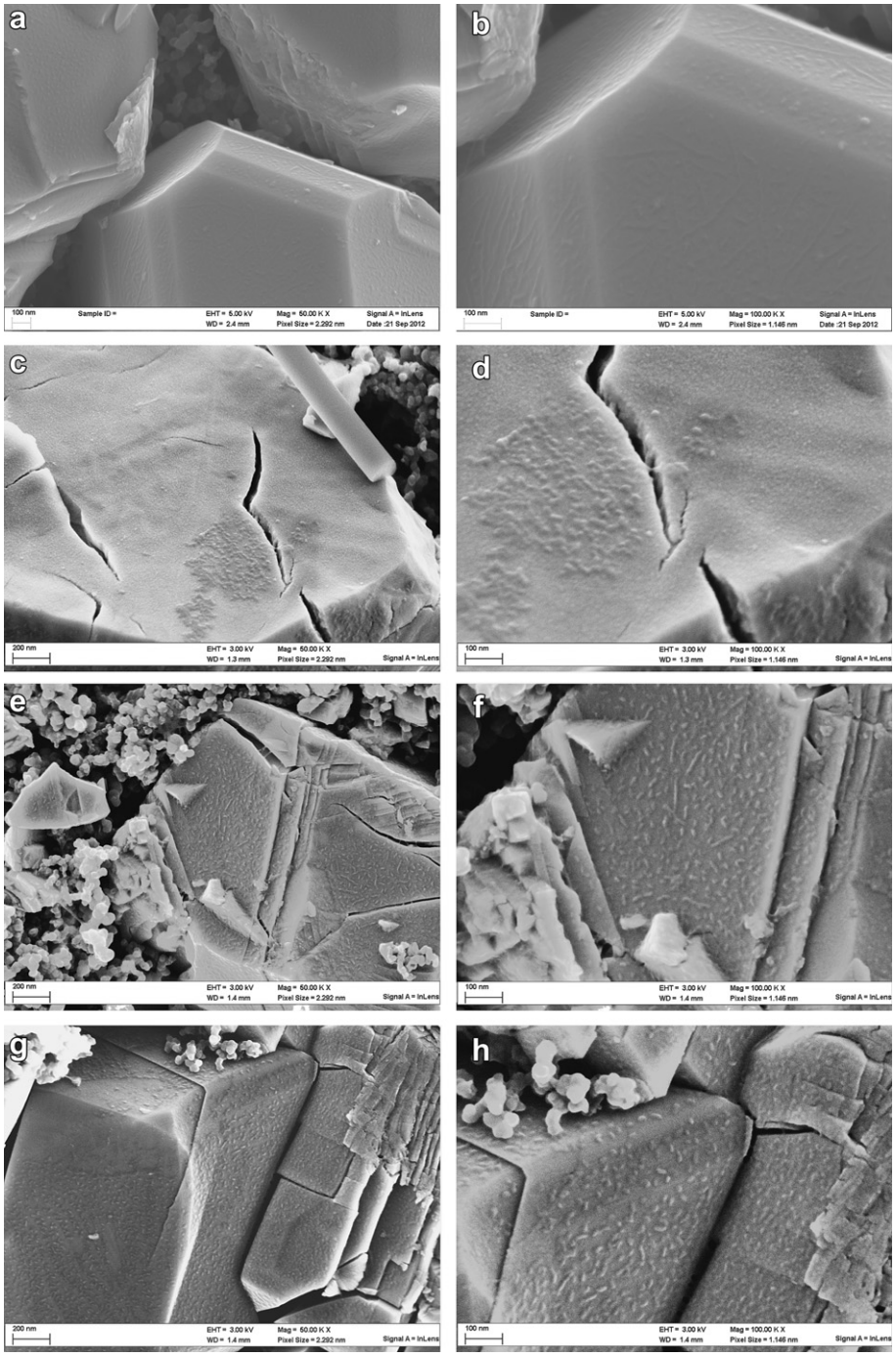

Fig. 9. HRSEM analysis of a) & b) pristine LNMO based electrodes (after calendaring) and cycled electrodes after 62 cycles at different C rates (c–h). Electrodes have been cycled using c) & d) pure LP30 as electrolyte, e) & f) LP30 and 4% of SA, and g) & h) LP30 and 8% of SA as electrolyte. For each sample two SEM images at different magnifications are presented.

particularly in Fig. 9c–e could not be detected to this extent, potentially resulting from the materials stress induced by the continuous (de-)lithiation of the LNMO host structure. However, particularly in the higher magnifications (Fig. 9b, d, f, h), a clearly differently structured surface of the LNMO particles is observed, resulting from the formation of a surface film upon cycling (Fig. 9d, f, h), which appears to be modified by the addition of 4% and 8% of SA to the base electrolyte (Fig. 9f, h).

In order to investigate the composition and particularly the differences in composition of this surface film when SA is added to the electrolyte, XPS analysis was performed. In Fig. 10 the XPS spectra for a pristine electrode (labeled as 'pristine'), an electrode galvanostatically cycled using pure LP30 as electrolyte ('LP30'), as well as electrodes cycled using LP30 as electrolyte, comprising 4 and 8 wt.% of SA as additive ('4% SA' and '8% SA'), are presented. The C 1s spectrum of the pristine LNMO based electrode shows the characteristic signals for amorphous carbon at 285 eV, originating from Super C65®, and two peaks at 286.9 eV and 291.0 eV, indicating the presence of $-CH_2$ or rather $-CF_2$ groups, corresponding to PVdF. The C 1s spectrum obtained for the electrode cycled in the

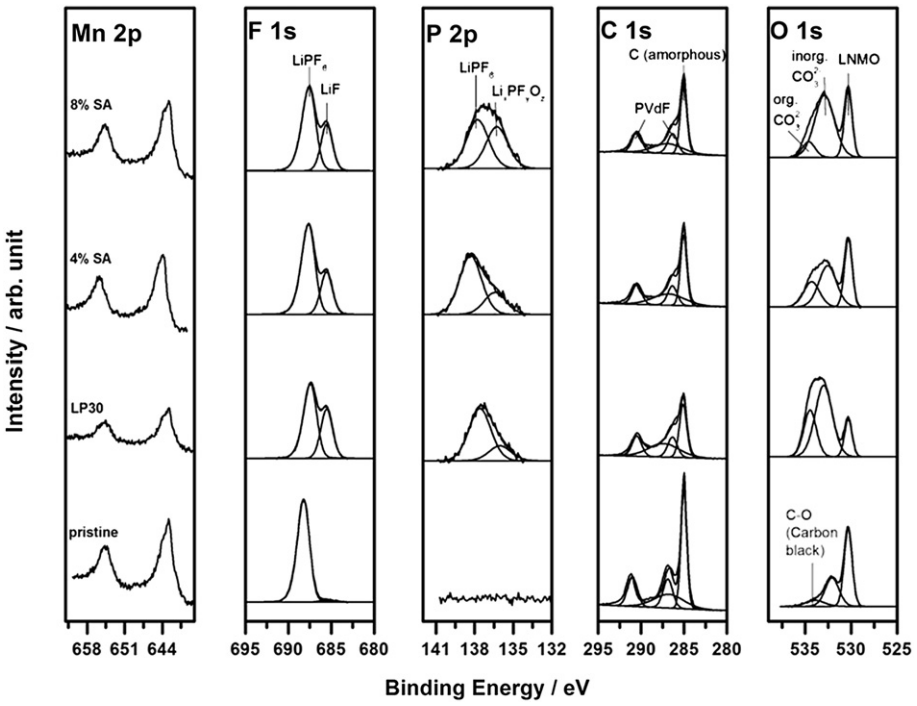

Fig. 10. XPS spectra of the Mn 2p, F 1s, P 2p, C 1s, and O 1s regions for pristine LNMO based electrodes as reference ('pristine') and cycled LNMO based electrodes using pure LP30 ('LP30') as electrolyte as well as LP30 comprising 4 wt.% ('4% SA') and 8 wt.% of SA ('8% SA') as electrolyte additive.

pure electrolyte ('LP30') reveals a significant decrease in peak intensity for all of these signals with respect to the pristine one. This can be explained by the formation of a surface layer on the cycled electrode caused by the oxidative electrolyte decomposition as already indicated by the electrochemical investigation of such electrodes. However, when SA is added into the electrolyte, the formation of such a surface layer appears to be less distinctive, as the intensity of the peaks decreases much less than for the pure electrolyte. Thus, it can be concluded that the addition of SA to the electrolyte leads to a decreased electrolyte decomposition, caused by the formation of a more stable SEI film on the LNMO particles, being in good agreement with the improved coulombic efficiency, the reduced capacity loss per cycle, as well as the decreased self-discharge upon storage at high potentials, according to the above discussed self-discharge mechanism and the importance of a stable and protective SEI to protect the cathode surface (Fig. 5).

In the O 1s spectrum of the pristine electrode, the characteristic peak for metal-oxide bonds (LNMO) at 530.3 eV is observed. Additionally, the presence of inorganic carbonates (532.1 eV), presumably Li_2CO_3, is revealed, resulting from the contact of the pristine electrodes with air (mainly carbon dioxide) and moisture [40–42] upon electrode preparation. Besides, a peak having a rather low intensity can be observed, which can be assigned to the presence of C–O bonds and might originate from surface groups on the conductive carbon [43,44]. Comparing now the O 1s spectra of cycled electrodes with that of the pristine electrode, it is obvious that the intensity of the peaks corresponding to the presence of inorganic and organic carbonates, as for instance poly(ethylene carbonate), significantly increases, indicating the oxidative decomposition of the electrolyte components at the cathode surface [32]. However, while the intensity of the peak corresponding to the presence of organic carbonate species decreases in the order 'LP30' > '4% SA' > '8% SA', the intensity of the peak corresponding to inorganic carbonate species decreases initially by adding 4% of SA to the electrolyte relatively to 'LP30', but increases by adding more SA ('8% SA'). If we suggest that the SEI formed on the LNMO particles is thinner for '4% SA' and '8% SA' relatively to 'LP30', as indicated by the higher intensity of the LNMO peak (O 1s), the PVdF peaks (C 1s), the carbon peak (C 1s), and the manganese peaks (Mn 2p), the composition appears to be clearly different. Han et al. [45] have reported a favored formation of Li_2CO_3 on silicon based anodes by adding SA to the electrolyte, which agrees well with the increase in intensity of peak related to the presence of inorganic carbonate species in Fig. 10 (O 1s). Additionally, they observed a reduced decomposition of $LiPF_6$, which is in accordance with the herein reported results (Fig. 10, F 1s). Moreover, the addition of SA leads to an increased formation of fluorophosphates (e.g. $Li_xPF_yO_z$, Fig. 10, P 2p, 136 eV) rather than LiF (Fig. 10, F 1s, 685.5 eV) as decomposition product of the lithium salt [46,47]. This is in good agreement with the results reported by Wang et al. [24], who investigated the effect of glutaric anhydride as additive on the LNMO/electrolyte interphase. As these fluorophosphates remained on the active materials surface after rinsing while LiF was mostly removed, they concluded that the addition of glutaric anhydride to the electrolyte resulted in a more stable and homogenous interphase. Furthermore, it is suggested that the reduced amount of LiF on the electrode surface leads to a less resistive interphase. It appears noteworthy at this point that the XPS analysis of non-rinsed electrodes entails the risk of including the detection of soluble species. Nevertheless, as reported by Wang et al. [24] a prior rinsing of the electrodes might result in a removal of less adhesive or slightly soluble interphase components, as for instance LiF, and thus to different conclusions regarding the modified composition of the surface film and accordingly, the effect of the electrolyte additive.

However, in order to clarify the detailed effect of succinic anhydride on the anodic electrolyte decomposition reaction, further investigation of the LNMO/electrolyte interphase as well as the liquid electrolyte by different analytical methods is currently performed in our laboratories and will hopefully allow further insight into the beneficial influence of succinic anhydride as electrolyte additive on the self-discharge of 5 V $LiNi_{0.4}Mn_{1.6}O_4$ cathodes.

4. Conclusions

The self-discharge mechanism of LNMO based cathodes was investigated by means of electrochemical methods and appeared fully reversible, resulting from the oxidative electrolyte decomposition at the LNMO surface. Based on these results 40 different compounds were investigated as suitable electrolyte additives to form a stable solid electrolyte interphase, preventing further electrolyte decomposition and thus, the occurring self-discharge upon storage. However, only succinic anhydride appeared to have a beneficial effect, lowering significantly the concomitant potential decay and capacity loss by up to more than 50%, while at the same time improving the coulombic efficiency as well as reducing the capacity loss per cycle.

In accordance with the electrochemical results, *ex situ* SEM and XPS analysis of cycled electrodes revealed a modified LNMO particles surface and the formation of a thinner, more stable SEI film on galvanostatically cycled electrodes by adding succinic anhydride to the base electrolyte.

Acknowledgment

Financial support from the European Commission within the AMELIE project (265910) under the Seventh Framework Programme (7th FWP) is gratefully acknowledged. Furthermore, the authors want to thank Mr. Steffen Krueger and Mr. Jan von Zamory for performing SEM and Dr. Sascha Nowak for performing ICP-OES analysis. Solvay SA is gratefully acknowledged for providing the PVdF-based copolymer Solef 5130 within the framework of the AMELIE project.

References

[1] K. Amine, H. Tukamoto, H. Yasuda, Y. Fujita, Journal of Power Sources 68 (1997) 604–608.
[2] Q.M. Zhong, A. Bonakdarpour, M. Zhang, Y. Gao, J.R. Dahn, Journal of the Electrochemical Society 144 (1997) 205–213.
[3] B. Scrosati, J. Garche, Journal of Power Sources 195 (2010) 2419–2430.
[4] J.B. Goodenough, Y. Kim, Chemistry of Materials 22 (2010) 587–603.
[5] A. Manthiram, Journal of Physical Chemistry Letters 2 (2011) 176–184.
[6] V. Etacheri, R. Marom, R. Elazari, G. Salitra, D. Aurbach, Energy & Environmental Science 4 (2011) 3243–3262.
[7] K.M. Shaju, P.G. Bruce, Dalton Transactions (2008) 5471–5475.
[8] S. Patoux, L. Sannier, H. Lignier, Y. Reynier, C. Bourbon, S. Jouanneau, F. Le Cras, S. Martinet, Electrochimica Acta 53 (2008) 4137–4145.
[9] J.-H. Kim, S.-T. Myung, C.S. Yoon, S.G. Kang, Y.-K. Sun, Chemistry of Materials 16 (2004) 906–914.
[10] S. Patoux, L. Daniel, C. Bourbon, H. Lignier, C. Pagano, F. Le Cras, S. Jouanneau, S. Martinet, Journal of Power Sources 189 (2009) 344–352.
[11] K. Xu, Chemical Reviews 104 (2004) 4303–4418.
[12] R. Yazami, Y. Ozawa, Journal of Power Sources 153 (2006) 251–257.
[13] R. Dedryvere, D. Foix, S. Franger, S. Patoux, L. Daniel, D. Gonbeau, The Journal of Physical Chemistry C 114 (2010) 10999–11008.
[14] E. Markevich, V. Baranchugov, D. Aurbach, Electrochemistry Communications 8 (2006) 1331–1334.
[15] Y.-K. Sun, Y.-S. Lee, M. Yoshio, K. Amine, Electrochemical and Solid-State Letters 5 (2002) A99–A102.
[16] S. Brutti, V. Gentili, P. Reale, L. Carbone, S. Panero, Journal of Power Sources 196 (2011) 9792–9799.
[17] R. Alcántara, M. Jaraba, P. Lavela, J.L. Tirado, Journal of Electroanalytical Chemistry 566 (2004) 187–192.
[18] H.M. Wu, I. Belharouak, A. Abouimrane, Y.-K. Sun, K. Amine, Journal of Power Sources 195 (2010) 2909–2913.
[19] T. Yang, N. Zhang, Y. Lang, K. Sun, Electrochimica Acta 56 (2011) 4058–4064.
[20] D. Liu, J. Trottier, P. Charest, J. Fréchette, A. Guerfi, A. Mauger, C.M. Julien, K. Zaghib, Journal of Power Sources 204 (2012) 127–132.
[21] S.S. Zhang, Journal of Power Sources 162 (2006) 1379–1394.
[22] A. von Cresce, K. Xu, Journal of the Electrochemical Society 158 (2011) A337–A342.
[23] S. Dalavi, M. Xu, B. Knight, B.L. Lucht, Electrochemical and Solid-State Letters 15 (2011) A28–A31.
[24] Z. Wang, N. Dupré, L. Lajaunie, P. Moreau, J.-F. Martin, L. Boutafa, S. Patoux, D. Guyomard, Journal of Power Sources 215 (2012) 170–178.
[25] H. Lee, S. Choi, S. Choi, H.-J. Kim, Y. Choi, S. Yoon, J.-J. Cho, Electrochemistry Communications 9 (2007) 801–806.
[26] J. Cabana, H. Zheng, A.K. Shukla, C. Kim, V.S. Battaglia, M. Kunduraci, Journal of the Electrochemical Society 158 (2011) A997–A1004.
[27] J. Mao, K. Dai, Y. Zhai, Electrochimica Acta 63 (2012) 381–390.
[28] D. Guyomard, J.M. Tarascon, Solid State Ionics 69 (1994) 222–237.
[29] G. Pistoia, A. Antonini, R. Rosati, D. Zane, Electrochimica Acta 41 (1996) 2683–2689.
[30] G. Pistoia, D. Zane, Y. Zhang, Journal of the Electrochemical Society 142 (1995) 2551–2557.
[31] J. Niu, B.E. Conway, W.G. Pell, Journal of Power Sources 135 (2004) 332–343.
[32] L. Yang, B. Ravdel, B.L. Lucht, Electrochemical and Solid-State Letters 13 (2010) A95–A97.
[33] S.E. Sloop, J.B. Kerr, K. Kinoshita, Journal of Power Sources 119–121 (2003) 330–337.
[34] R. Yazami, Electrochimica Acta 45 (1999) 87–97.
[35] S. Flandrois, B. Simon, CARBON – American Carbon Committee 37 (1999) 165–180.
[36] H. Duncan, Y. Abu-Lebdeh, I.J. Davidson, Journal of the Electrochemical Society 157 (2010) A528–A535.
[37] D. Guyomard, J.M. Tarascon, Journal of the Electrochemical Society 139 (1992) 937–948.
[38] D. Guyomard, J.M. Tarascon, Journal of the Electrochemical Society 140 (1993) 3071–3081.
[39] K. Kanamura, Journal of Power Sources 81–82 (1999) 123–129.
[40] W. Li, B.L. Lucht, Journal of the Electrochemical Society 153 (2006) A1617–A1625.
[41] M. Hirayama, N. Sonoyama, M. Ito, M. Minoura, D. Mori, A. Yamada, K. Tamura, J. Mizuki, R. Kanno, Journal of the Electrochemical Society 154 (2007) A1065–A1072.
[42] M. Hirayama, H. Ido, K. Kim, W. Cho, K. Tamura, J. Mizuki, R. Kanno, Journal of the American Chemical Society 132 (2010) 15268–15276.
[43] D. Pantea, H. Darmstadt, S. Kaliaguine, L. Sümmchen, C. Roy, Carbon 39 (2001) 1147–1158.
[44] M.E. Spahr, D. Goers, A. Leone, S. Stallone, E. Grivei, Journal of Power Sources 196 (2011) 3404–3413.
[45] G.-B. Han, M.-H. Ryou, K.Y. Cho, Y.M. Lee, J.-K. Park, Journal of Power Sources 195 (2010) 3709–3714.
[46] C.L. Campion, W. Li, B.L. Lucht, Journal of the Electrochemical Society 152 (2005) A2327–A2334.
[47] S. Verdier, L. El Ouatani, R. Dedryvère, F. Bonhomme, P. Biensan, D. Gonbeau, Journal of the Electrochemical Society 154 (2007) A1088–A1099.
[48] Y.-K. Han, J. Jung, S. Yu, H. Lee, Journal of Power Sources 187 (2009) 581–585.